Distinguishing between void models and dark energy with cosmic parallax and redshift drift

Miguel Quartin[1,*] and Luca Amendola[1,2,*]

[1]*Institut für Theoretische Physik, Universität Heidelberg, Philosophenweg 16, 69120 Heidelberg, Germany*
[2]*INAF/Osservatorio Astronomico di Roma, V. Frascati 33, 00040 Monteporzio Catone, Roma, Italy*

Two recently proposed techniques, involving the measurement of the cosmic parallax and redshift drift, provide novel ways of directly probing (over a time span of several years) the background metric of the universe and therefore shed light on the dark-energy conundrum. The former makes use of upcoming high-precision astrometry measurements to either observe or put tight constraints on cosmological anisotropy for off-center observers, while the latter employs high-precision spectroscopy to give an independent test of the present acceleration of the universe. In this paper, we show that both methods can break the degeneracy between Lemaître-Tolman-Bondi void models and more traditional dark-energy theories. Using the near-future observational missions Gaia and CODEX we show that this distinction might be made with high confidence levels in the course of a decade.

I. INTRODUCTION

The enigma of the cosmic acceleration has solicited explanations that range from new matter components with negative pressure, to modifications of gravity, to large-scale violations of the cosmological principle of homogeneity and isotropy. The latter class of models is probably the most controversial but has the merit of linking explicitly the acceleration (apparent or real) to the formation of nonlinear structures and of dispensing with unknown and so far unseen new cosmic components.

Any violation of the cosmological principle means that the simple structure of the Friedman-Robertson-Walker (FRW) metric can no longer be adopted, not even approximately, as a description of the universe properties. The simplest possibility is to adopt in place of the FRW metric the spherically symmetric structure of the Lemaître-Tolman-Bondi (LTB) metric, as suggested by various authors (e.g. [1–4]) ever since the discovery of acceleration (a similar but non-LTB void model was also investigated in [5]). In order to reproduce the accelerated expansion, the LTB structure must allow for a faster expansion inside than outside, which is generally (although not necessarily [6]) obtained by a radial density profile that generate a huge ($\approx$ 1–2 Gpc) void. Notice that in this case the observed supernovae acceleration is not real but rather due to the comparison of different sources (inside and outside the void) and to the assumption of homogeneity; in reality, in a LTB universe composed uniquely by dust matter there is no real acceleration, except possibly (i.e., depending on the density profile model) near the edge. Although a single huge LTB bubble with the Milky Way right near the center is undoubtedly a contrived configuration, this can be thought of as a first approximation towards a more realistic model,

for instance a collection of ellipsoidal voids and "meatballs" of different sizes [7–9]. In any case, almost all other dark-energy models suffer from high-degrees of fine-tuning, either in the necessary initial conditions or in the form of the coincidence problem [10,11].

As we discuss in more detail in the next section, the LTB metric allows for two spatial degrees of freedom, that could be employed to reproduce any line-of-sight expansion rate and any line-of-sight inhomogeneity. In particular, LTB models (although not necessarily voids) can mimic the observed accelerated expansion rate $H(z)$ and the observed source number counts at the same time [6,12,13]. Because of this flexibility, and because of the isotropy with respect to the center observer, ruling out the LTB model is not a trivial task.

Although we sometimes take for granted that in cosmology we can only access the surface of a single light cone, this is by no means true. We can in fact receive CMB light scattered from distant sources, for instance from the hot intracluster medium of galaxy clusters through the Sunyaev-Zel'dovich effect, which comes from inside our light cone. The spectrum of these scattered CMB photons will be distorted from their original blackbody spectrum and the amount of deviation is proportional to the peculiar velocity of the cluster with respect to the CMB scattering surface [14]. This effect can be employed to map the cosmic peculiar velocity field and therefore adds to the expansion rate and the number counts a third spatial function that can break the fundamental degeneracy of LTB and FRW. Similarly, since during reionization the CMB photons are scattered towards us by structures that are located off-center, their spectrum will be the sum of blackbody spectra at different temperatures and therefore will again deviate from a blackbody spectrum [15]. The amount of deviation depends on the distance with respect to the center and provides again an additional piece of information that can break the degeneracy.

---

*m.quartin@thphys.uni-heidelberg.de
† l.amendola@thphys.uni-heidelberg.de

In the above two examples one receives information from inside our own light cone making use of sources along it. Two additional techniques recently proposed explore instead the *exterior* of our present light cone by observing the same sources at two different instants of time. In other words, by probing two or more different (albeit very close) light cones.

The first method relies on high-precision spectroscopy. If the time-span Δt is large enough, one can detect small changes $\Delta_t z$ in the source redshift proportional to the local expansion rate: this is the so-called Sandage effect [16] or redshift drift [17,18]. As we will show below, the redshift drift can be used to distinguish between real acceleration driven by dark energy ($\Delta_t z > 0$) and apparent acceleration ($\Delta_t z < 0$). This technique has been presented on a general basis in [12,19] but never discussed in any detail nor compared to dark-energy cosmologies.

The second method requires high-precision astrometry and exploits the fact that off-center observers see an anisotropic space. We already know that the distance from the LTB center is limited to less than 50–100 Mpc/h by the observed isotropy of the CMB, of number counts and of the supernovae Hubble diagram. It is however possible to considerably reduce this upper limit by exploiting the recently proposed cosmic parallax (CP) effect [20–23]. The CP is the change in the angular separation of distant sources induced by the differential expansion rate in anisotropic universes. Any off-center observer in a LTB void will experience an anisotropic expansion and therefore a CP, proportional (at first order) to the distance from the void center. In [20] this was applied to voids and in [22,23] to Bianchi I models.

The redshift drift and the cosmic parallax form a new set of real-time cosmic observables. In this paper we discuss both methods. In particular, we calculate the former in the case of an LTB void and show that, with the proposed E-ELT instrument CODEX [24], it is one of the most promising way to distinguish voids from standard dark-energy models. For the cosmic parallax, we generalize and improve on a number of points the previous treatments: we extend the analytical estimates for sources at arbitrary positions, make a more accurate estimate of the observational power of both Gaia [25,26] and the SIM Lite Astrometric Observatory [27,28] missions using a realistic quasar distribution (taking into account two major systematics), investigate the redshift dependence of both signal and noise and propose a possible Figure of Merit for future astrometry missions. We also include a third void model from the literature [4] to better understand the model-dependence of both real-time cosmic observables studied herein.

II. LTB VOID MODELS

The LTB metric can be written as (primes and dots refer to partial space and time derivatives, respectively):

$$ds^2 = -dt^2 + \frac{[R'(t,r)]^2}{1 + \beta(r)}dr^2 + R^2(t,r)d\Omega^2, \tag{1}$$

where $\beta(r)$ can be loosely thought as position dependent spatial curvature term. Two distinct Hubble parameters corresponding to the radial and perpendicular directions of expansion are defined as

$$H_\parallel = \dot{R}'/R', \tag{2}$$

$$H_\perp = \dot{R}/R. \tag{3}$$

Note that in a FRW metric $R = ra(t)$ and $H_\parallel = H_\perp$. The Einstein equations for pressureless matter reduce to

$$H_\perp^2 + 2H_\parallel H_\perp - \frac{\beta}{R^2} - \frac{\beta'}{RR'} = 8\pi G\rho_m, \tag{4}$$

$$6\frac{\ddot{R}}{R} + 2H_\perp^2 - 2\frac{\beta}{R^2} - 2H_\parallel H_\perp + \frac{\beta'}{RR'} = -8\pi G\rho_m. \tag{5}$$

They can be further summed into a single equation which can be integrated once to give the classical cycloid equations

$$H_\perp^2 = \frac{\alpha(r)}{R^3} + \frac{\beta(r)}{R^2}, \tag{6}$$

where $\alpha(r)$ is a free function that we can use along with $\beta(r)$ to describe the inhomogeneity. From this we can define an effective density parameter $\Omega_{m0}(r) = \Omega_m(r, t_0)$ today:

$$\Omega_{m0}(r) \equiv \frac{\alpha(r)}{R_0^3 H_{\perp,0}^2}, \tag{7}$$

where $R_0 \equiv R(r, t_0)$, $H_{\perp,0} \equiv H_\perp^2(r, t_0)$ and an effective spatial curvature

$$\Omega_{K0}(r) = 1 - \Omega_{m0}(r) = \frac{\beta(r)}{R_0^2 H_{\perp,0}^2}. \tag{8}$$

Note there another possible (and nonequivalent) definition is sometimes found in the literature [3]. Equation (6) is the classical cycloid equation whose solution for $\beta > 0$ is given parametrically by

$$R(r, \eta) = \frac{\alpha(r)}{2\beta(r)}(\cosh\eta - 1)$$
$$= \frac{R_0 \Omega_{m0}(r)}{2[1 - \Omega_{m0}(r)]}(\cosh\eta - 1), \tag{9}$$

$$t(r, \eta) - t_B(r) = \frac{\alpha(r)}{2\beta^{3/2}(r)}(\sinh\eta - \eta)$$
$$= \frac{\Omega_{m0}(r)}{2[1 - \Omega_{m0}(r)]^{3/2}H_{\perp,0}}(\sinh\eta - \eta), \tag{10}$$

where the "time" variable η is defined by the relation

$$\partial \eta / \partial t = R^{-1} \beta^{1/2}, \tag{11}$$

and where $t_B(r)$ is another free spatial function. The universe age $T(r)$ corresponds to the time past since big-bang $R(r, \eta = 0) = 0$ at distance r from the center and amounts to

$$T = t_0 - t_B = \frac{1}{H_{\perp,0}} \left[\frac{1}{\Omega_{K0}} - \frac{\Omega_{m0}}{(\Omega_{K0})^{3/2}} \operatorname{arcsinh} \sqrt{\frac{\Omega_{K0}}{\Omega_{m0}}} \right], \tag{12}$$

where t_0 is the present time. Of the four free spatial functions that determine the solution, $t_B(r)$, R_0, $\Omega_{m0}(r)$ and $H_{\perp,0}$, two can be fixed arbitrarily by a redefinition of r and t. Henceforth, following most of the literature, we choose $R_0 = r$ and $t_B(r) = 0$, i.e., adopt the same function that reproduces the FRW limit at the present epoch and synchronize the clocks at big-bang time. The two remaining degrees of freedom can be expressed equivalently by $\Omega_{m0}(r)$, $H_{\perp 0}$ or by $\alpha(r)$, $\beta(r)$ or other combinations. So we can write the relation

$$\alpha(r) = R_0^3 H_{\perp 0}^2 \Omega_{m0} \tag{13}$$

$$\beta(r) = R_0^2 H_{\perp 0}^2 (1 - \Omega_{m0}), \tag{14}$$

useful to convert models given in literature into one another. Fixing the cosmic age $T(r)$ to be spatially homogeneous, one eliminates yet another degree of freedom leaving only one free function. This also ensures that there are no huge inhomogeneities in the past. For simplicity, all the models we use below are chosen to have homogeneous cosmic age but this choice plays no special role in what concerns our analysis.

A. Current constraints on void models

Void models have been studied quite intensively in the last few years and several ideas have been put forward to constrain their properties. We mentioned already the possibility of constraints due to spectral distortions induced by scattered CMB light either from reionized regions [15] or by the hot intracluster medium [14]. The current data constrain the void size to be no larger than 1–2 Gigaparsecs, although with a strong dependence on the central density and the profile. In any case, voids this large are still a good fit of the supernovae data (see e.g. the recent analyses of Refs. [29–31]).

Since in general we have two free functions, we need two independent observables to reconstruct the void profile. The number density data are heavily subject to evolution, selection and bias effects, so probably the most promising method is to combine the estimation of angular or luminosity distances (provided by supernovae or baryon acoustic oscillations) with a direct measure of the expansion rate $H(z)$ given by longitudinal baryon acoustic oscillations [32], as suggested in [31].

B. Off-center observers

Although most authors consider the observers to be at the center of symmetry of the LTB void for simplicity, there is no *a priori* reason for that and one should consider the possibility of off-center observers. This has been done in [33,34] and it was shown that supernovae and the size of the CMB dipole limit such a displacement to around 150 [34] and 15 Mpc [33] (in terms of the physical distance), respectively. Actually, as will be shown, a more accurate limit on the latter case is 26 Mpc, and a recent analysis showed that supernovae constraints may be a little looser [35]. Nevertheless the current tightest constraints on void-induced anisotropies come from the CMB dipole.

However, in order to derive such a limit one has to assume that the observer has no relative velocity relative to the surface of last scattering. In other words, the CMB dipole would be completely due to the off-center displacement. This is in direct contrast to the standard FRW scenario, where the dipole is almost completely due to our own peculiar velocity. If on the other hand the off-center observer in LTB has a peculiar velocity, then the maximum off-center distance can vary substantially. A good estimation of this limit can be done following [33] through a simplified Newtonian picture, which was numerically confirmed to give very good description.

The measured CMB dipole is 3.358 ± 0.023 mK [36], which when compared to the average CMB temperature of 2.725 K gives a temperature contrast Θ with an amplitude of 0.0012. If the dipole is due only to the off-center displacement, one can write (in the usual spherical harmonics decomposition)

$$\Theta^{\mathrm{dipole}} = a_{10} Y_{10}, \tag{15}$$

from which one gets $a_{10} = 2.5 \cdot 10^{-3}$ (note that in this case a_{11} and a_{1-1} are both zero [33]). The LTB off-center dipole seen by an observer at a physical distance X_{obs}, when compared to the homogeneous FRW case with a spatially constant Hubble parameter h^{out}, can be understood as an equivalent "peculiar velocity" of roughly

$$\beta_v \equiv \frac{v_p}{c} = \frac{h^{\mathrm{in}} - h^{\mathrm{out}}}{3000 \text{ Mpc}} X_{\mathrm{obs}} \tag{16}$$

with respect to the origin. In such a picture, the temperature anisotropies measured by the observer are attributed to a Doppler shift of the CMB photons due to his motion. In this picture it was shown [33] that the dipole scales linearly, the quadrupole quadratically, and the octopole cubically with the observers position. The expressions for the dipole to the lowest order in β_v is

$$a_{10} = \sqrt{\frac{4\pi}{3}} \frac{h^{\mathrm{in}} - h^{\mathrm{out}}}{3000 \text{ Mpc}} X_{\mathrm{obs}}. \tag{17}$$

From this approximation one gets that the maximum off-center physical distance is 26 Mpc.

This Newtonian picture is also very useful if we want to consider both effects at the same time: an off-center distance and a (real) peculiar velocity of the observer. Without a real peculiar velocity, (16) gives $\beta_v = 373$ km/s, which not surprisingly is very close to the CMB inferred velocity between the Sun and the CMB in a standard FRW metric. If one now considers a typical (real) peculiar velocity of 500 km/s in the LTB case it is easy to see from (16) that if this velocity is in the direction of the LTB center, one can have an effective $\beta_v^{\text{eff}} = 873$ km/s, which pushes back the maximum off-center physical distance to a little more that 60 Mpc. Of course we have no reason to believe that such an alignment should exist, but neither do we currently possess any observations that could break such a degeneracy. In other words, although not likely, an off-center distance of 60 Mpc cannot currently be ruled out.[1] Nevertheless, in order to separate both void-induced and velocity-induced effects, we will not push for such an aggressive off-center distance and henceforth we will assume as the fiducial displacement a more conservative value of 30 Mpc (although we will come back to this point in Sec. V).

III. COSMIC PARALLAX AND REDSHIFT DRIFT IN LTB

A. Estimating the parallax for general anisotropy

Figure 1 depicts the overall scheme describing a possible time-variation of the angular position of a pair of sources that expand anisotropically with respect to the observer. We label the two sources a and b, and the two observation times 1 and 2. In what follows, we will refer to (t, r, θ, ϕ) as the comoving coordinates with origin on the center of a spherically symmetric model. Peculiar velocities apart, the symmetry of such a model forces objects to expand radially outwards, keeping r, θ, and ϕ constant.

Let us assume now an expansion in a flat FRW space from a "center" C observed by an off-center observer O at a distance X_{obs} from C. Since we are assuming FRW it is clear that any point in space could be considered a center of expansion: it is only when we will consider a LTB universe that the center acquires an absolute meaning. The relation between the observer line-of-sight angle ξ and the coordinates of a source located at a radial distance X and angle θ in the C-frame is

$$\cos\xi = \frac{X\cos\theta - X_{\text{obs}}}{(X^2 + X_{\text{obs}}^2 - 2X_{\text{obs}}X\cos\theta)^{1/2}}, \quad (18)$$

where all angles are measured with respect to the CO axis

---

[1] In fact, a higher peculiar velocity of, say, 1000 km/s could stretch this value to almost 100 Mpc, after which other anisotropical constraints such as the ones coming from supernovae are likely to be more stringent.
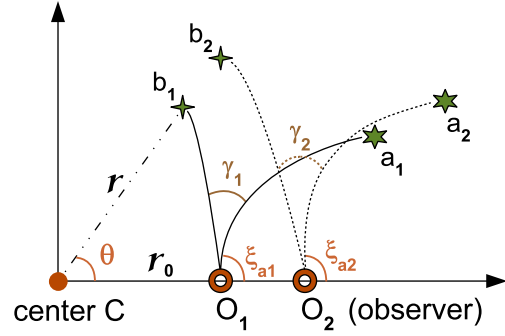

FIG. 1 (color online). Overview, notation and conventions of the cosmic parallax effect. Note that for clarity purposes we assumed here that the points C, O_1, a_1, b_1 all lie on the same plane. By symmetry, points O_2, a_2, b_2 remain on this plane as well. Comoving coordinates r and r_{obs} correspond to physical coordinates X and X_{obs}.

and all distances in this section are to be understood as physical distances. Through most of this paper we shall assume for simplicity (and clarity) that both sources share the same ϕ coordinate.

We consider first two sources at location a_1, b_1 on the same plane that includes the CO axis with an angular separation γ_1 as seen from O, both at distance X from C. After some time Δt, the sources move to positions a_2, b_2 and the distances X and X_{obs} will have increased by $\Delta_t X$ and $\Delta_t X_{\text{obs}}$ respectively, so that the sources subtend an angle γ_2. In a FRW universe, these increments are such that they keep the overall separation γ constant. However, if for a moment we allow ourselves the liberty of assigning to the scale factor $a(t)$ and the H function a spatial dependence, a time-variation of γ is induced. The variation

$$\Delta_t \gamma \equiv \gamma_1 - \gamma_2 \quad (19)$$

is the cosmic parallax effect and can be easily estimated if we suppose that the Hubble law is just generalized to

$$\Delta_t X = XH(t_0, X)\Delta t \equiv XH_X\Delta t, \quad (20)$$

where

$$X(r) \equiv \int^r g_{rr}^{1/2} dr' = \int^r a(t_0, r')dr', \quad (21)$$

generalizes the FRW relation $X_{\text{FRW}} = a(t_0)r$ in a metric whose radial coefficient is g_{rr}.

For two arbitrary sources at distances much larger than X_{obs}, after straightforward geometry we arrive at

$$\Delta_t \gamma = \Delta t (H_{\text{obs}} - H_X)X_{\text{obs}}\left[\frac{\sin\theta_a}{X_a} - \frac{\sin\theta_b}{X_b}\right]. \quad (22)$$

For sources on similar shells, i.e., separated by a small $\Delta X \equiv X_b - X_a$ (not to be mistaken with the *time* interval $\Delta_t X$), we can write

$$\Delta_t\gamma \simeq s\Delta t(H_{\mathrm{obs}} - H_X)\left[\sin\theta_a - \sin\theta_b\left(1 - \frac{\Delta X}{X}\right)\right], \quad (23)$$

where we dropped the index "a" on X, $H_{\mathrm{obs}} \equiv H(t_0, r_{\mathrm{obs}})$ and we defined the parameter

$$s \equiv \frac{X_{\mathrm{obs}}}{X} \ll 1. \quad (24)$$

The above analytical estimates have been verified numerically, and the angular dependence of the CP for sources at similar distances has been verified to hold to very high precision.

The signal $\Delta_t\gamma$ in (23) depends on both source angles $\theta_{a,b}$. We can average over $\theta_{a,b}$ to obtain the average cosmic parallax for two arbitrary sources in the sky (still assuming they lie on the same plane that contains CO). If both sources are at the same redshift, then the average CP effect is given by

$$\langle\Delta_t\gamma\rangle_{\mathrm{perp}} \simeq \frac{s\Delta t(H_{\mathrm{obs}} - H_X)}{4\pi^2}\int_0^{2\pi}\int_0^{2\pi}|\sin\theta_a$$
$$- \sin\theta_b|d\theta_a d\theta_b \quad (25)$$

$$= \frac{8}{\pi^2}s\Delta t(H_{\mathrm{obs}} - H_X). \quad (26)$$

Note that at this order we can neglect the difference between the observed angle ξ and θ. We can also convert the above intervals ΔX into the redshift interval Δz by using the relation $r = \int dz/H(z)$. Using (21) we can write $\Delta X = a(t_0, X)\Delta z/H(z) \sim \Delta z/H(z)$ (we impose the normalization $a(t_0, X_{\mathrm{obs}}) = 1$), where $H(z) \equiv H(t(z), X)$. One should note that in a non-FRW metric, one has $s \neq r_0/r$.

In a FRW metric, H does not depend on r and the parallax vanishes. On the other hand, any deviation from FRW entails such spatial dependence and the emergence of cosmic parallax, except possibly for special observers (such as the center of LTB). A constraint on $\Delta_t\gamma$ is therefore a constraint on cosmic anisotropy.

Rigorously, the use of the above equations is inconsistent outside a flat FRW scenario; one actually needs to perform a full integration of light-ray geodesics in the new metric. Nevertheless, we shall assume for a moment that for an order of magnitude estimate we can simply replace H with its space-dependent counterpart given by LTB models. In order for an alternative LTB cosmology to have any substantial effect (e.g., explaining the SNIa Hubble diagram) it is reasonable to assume a difference between the local H_{obs} and the distant H_X of order H_{obs} [33]. More precisely, putting $H_{\mathrm{obs}} - H_X = H_{\mathrm{obs}}\Delta h$ then using (25) one has that the average $\Delta_t\gamma$ is of order

$$\langle\Delta_t\gamma\rangle|_{\mathrm{perp}} \sim 20s\Delta h \ \mu\mathrm{as/year} \quad (27)$$

for two sources at the same redshift. Similarly, for source pairs at same position θ but different (yet similar) redshifts

one has [using (23)]

$$\Delta_t\gamma|_{\mathrm{rad}} \sim s\sin\theta\Delta h\Delta t\Delta z/X \ \mu\mathrm{as/year}$$
$$\sim 20s\sin\theta\Delta h\frac{\Delta z}{z} \ \mu\mathrm{as/year}, \quad (28)$$

where it was assumed that $X \sim zH(z)^{-1}$. The average radial CP for sources between 10 and 200 times X_{obs} can be obtained numerically to be

$$\langle\Delta_t\gamma\rangle_{\mathrm{rad}} \simeq \frac{\Delta t(H_{\mathrm{obs}} - H_X)\sin\theta}{190^2}$$
$$\times \int_{10}^{200}\int_{10}^{200}\left|\frac{1}{s_a} - \frac{1}{s_b}\right|d(1/s_a)d(1/s_b) \quad (29)$$

$$= 0.014\sin\theta\Delta t(H_{\mathrm{obs}} - H_X). \quad (30)$$

Therefore, one can estimate for the radial signal

$$\langle\Delta_t\gamma\rangle|_{\mathrm{rad}} \sim 0.3\sin\theta\Delta h \ \mu\mathrm{as/year}, \quad (31)$$

which is very similar to its same-shell counterpart (27), except for the $\sin\theta$ modulation.

Let us finally consider the main expected source of noise, the intrinsic peculiar velocities of the sources. The variation in angular separation for sources at angular diameter distance D_A (measured by the observer) and peculiar velocity v_{pec} can be estimated as

$$\Delta_t\gamma_{\mathrm{pec}} = \left(\frac{v_{\mathrm{pec}}}{500 \ \frac{\mathrm{km}}{\mathrm{s}}}\right)\left(\frac{D_A}{1 \ \mathrm{Gpc}}\right)^{-1}\left(\frac{\Delta t}{10 \ \mathrm{years}}\right) \ \mu\mathrm{as}. \quad (32)$$

This velocity field noise is therefore typically smaller than the experimental uncertainty (especially for large distances) and again will be averaged out for many sources. Notice that the observer's own peculiar velocity produces a systematic offset sinusoidal signal $\Delta_t\gamma_{\mathrm{pec},O}$ of the same amplitude as $\Delta_t\gamma_{\mathrm{pec}}$ that has to be subtracted from the observations: we discuss this further below. The above relation was further investigated in [21], where it was proposed to estimate D_A via observations of $\Delta_t\gamma_{\mathrm{pec}}$ due not to voids but by our motion with respect to the CMB.

B. Geodesic equations

As suggestive as the above estimates be, they need confirmation from an exact treatment where the full relativistic propagation of light rays is taken into account. We will thus consider in what follows three particular LTB models capable of fitting the observed SNIa Hubble diagram and the CMB first peak position and compatible with the COBE results of the CMB dipole anisotropy, as long as the observer is within around 30 Mpc from the center [33]. Moreover, all three models have void sizes which, although huge by any means, are "small" enough ($z \sim 0.3$–0.4) not to be ruled out due to distortions of the CMB blackbody radiation spectrum [15].

Because of the axial symmetry and the fact that photons follow a path which preserves the 4-velocity identity $u^\alpha u_\alpha = 0$, the 4 second-order geodesic equations for (t, r, θ, ϕ),

$$\frac{d^2 x^a}{d\lambda^2} + \Gamma^a_{bc} \frac{dx^b}{d\lambda} \frac{dx^c}{d\lambda} = 0, \qquad (33)$$

can be written as five first-order ones. Here λ is the arbitrary affine parameter of the geodesics. We will choose as variables the center-based coordinates t, r, θ, $p \equiv dr/d\lambda$ and the redshift z. We shall refer also to the conserved angular momentum

$$J \equiv R^2 \frac{d\theta}{d\lambda} = \text{const} = J_0, \qquad (34)$$

which is a direct consequence of the $a \to \theta$ equation in (33). For a particular source, the angle ξ is the coordinate equivalent to θ for the observer, and in particular ξ_0 is the coordinate ξ of a photon that arrives at the observer at the time of observation t_0. Obviously this coincides with the measured position in the sky of such a source at t_0. In terms of these variables, and defining λ such that $u(\lambda) < 0$, the autonomous system governing the geodesics is written as (see [33])

$$\frac{dt}{d\lambda} = -\sqrt{\frac{(R')^2}{1+\beta} p^2 + \frac{J^2}{R^2}}, \qquad \frac{dr}{d\lambda} = p, \qquad \frac{d\theta}{d\lambda} = \frac{J}{R^2},$$

$$\frac{dz}{d\lambda} = \frac{(1+z)}{\sqrt{\frac{(R')^2}{1+\beta} p^2 + \frac{J^2}{R^2}}} \left[\frac{R' \dot{R}'}{1+\beta} p^2 + \frac{\dot{R}}{R^3} J^2 \right],$$

$$\frac{dp}{d\lambda} = 2\dot{R}' p \sqrt{\frac{p^2}{1+\beta} + \frac{J^2}{R^2 R'^2}} + \frac{1+\beta}{R^3 R'} J^2$$

$$+ \left[\frac{\beta'}{2+2\beta} - \frac{R''}{R'} \right] p^2. \qquad (35)$$

The angle ξ along a geodesic is given by [33]:

$$\cos\xi = -\frac{R'(t,r) p}{u\sqrt{1+\beta(r)}}, \qquad (36)$$

from which we obtain, exploiting the remaining freedom in the definition of λ, the relations [33]

$$p_0 = -\frac{\sqrt{1+\beta(r_{\text{obs}})}}{R'(t_0, r_{\text{obs}})} \cos(\xi_0), \qquad (37)$$

$$J_0 = J = R(t_0, r_{\text{obs}}) \sin(\xi_0). \qquad (38)$$

Therefore, our autonomous system is completely defined by the initial conditions t_0, r_{obs}, $\theta_0 = 0$, $z_0 = 0$ and ξ_0. The first two define the instant of measurement and the offset between observer and center, while ξ_0 stands for the direction of incidence of the photons.

An algorithm for predicting the variation of an arbitrary angular separation can be written as follows:

(1) Denote with $(z_{a1}, z_{b1}, \xi_{a1}, \xi_{b1})$ the observed coordinate of a pair of sources at a given time t_0 and observer position r_{obs};

(2) Solve numerically the autonomous system with initial conditions $(t_0, r_{\text{obs}}, \theta_0 = 0, z_0 = 0, \xi_0 = \xi_{a1})$ and find out the values of λ_a^* such that $z(\lambda_a^*) = z_{a1}$;

(3) Take note of the values $r_{a1}(\lambda_a^*)$ and $\theta_{a1}(\lambda_a^*)$ (since the sources are assumed comoving with no peculiar velocities, these values are constant in time);

(4) Define $\lambda_a^\dagger$ as the parameter value for which $r_{a2}(\lambda_a^\dagger) = r_{a1}(\lambda_a^*)$, where r_{a2} is the geodesic solution for a photon arriving Δt later with an incident angle ξ_{a2}, and vary ξ_{a2} until $\theta_{a2}(\lambda_a^\dagger) = \theta_{a1}(\lambda_a^*)$;

(5) Repeat the above steps for source b, and compute the difference $\Delta_t \gamma \equiv \gamma_2 - \gamma_1 = (\xi_{a2} - \xi_{b2}) - (\xi_{a1} - \xi_{b1})$.

The above algorithm gives as a by-product another interesting observable, the Sandage redshift drift [16,17] (see Sec. III D). It is important to realize that the redshift drift is inherently coupled to the CP, that is, in principle one cannot calculate one effect without taking the other into account. A general prescription on how to obtain $\dot{z}$ for an observer at the center of a LTB model was obtained in [18]. As we will show in Sec. III E, in the limit of small s our numerical results reveal that $\Delta_t z$ for off-center observers show small angular dependence, and therefore to good approximation one can neglect the CP effect when calculating the redshift drift.

A remark on the above procedure is in order before we continue. Because of the intrinsically smallness of both the cosmic parallax and Sandage effects (in the course of a decade), a carefully constructed numerical code is needed to correctly compute either. To give an idea of the amount of precision required, consider the following: if one naively calculates $\Delta_t \gamma$ for a Δt of 10 years, one needs to evaluate ξ_{a1} and ξ_{a2} with at least 13 digits of precision (as the CP is of the order of 0.2 μas $\sim 10^{-12}$ rad). Although it is possible to alleviate this by exploiting the linearity of $\Delta_t \gamma$ in Δt and scaling up the system, it still remains a numerically challenging problem, as was independently found out in [22]. In Appendix A we explore this issue in more detail and describe how we were able to circumvent it in both the present and original paper [20].

C. Specific models

The models of Refs. [33,34] are characterized by a smooth transition between an inner void and an outer region with higher matter density and described by the functions:

$$\alpha(r) = (H^{\text{out}}_{\perp,0})^2 r^3 \left[1 - \frac{\Delta\alpha}{2} \left(1 - \tanh\frac{r - r_{\text{vo}}}{2\Delta r} \right) \right], \qquad (39)$$

$$\beta(r) = (H^{\text{out}}_{\perp,0})^2 r^2 \frac{\Delta\alpha}{2} \left(1 - \tanh\frac{r - r_{\text{vo}}}{2\Delta r} \right), \qquad (40)$$

where $\Delta\alpha$, r_{vo} and Δr are three free parameters and $H_{\perp,0}^{\mathrm{out}}$ is the Hubble constant at the outer region, set at $51 \ \mathrm{km}\,\mathrm{s}^{-1}\,\mathrm{Mpc}^{-1}$.

We will dub the two Models I and II, and define them by the sets $\{\Delta\alpha = 0.9, r_{\mathrm{vo}} = 1.46 \ \mathrm{Gpc}, \Delta r = 0.4 r_{\mathrm{vo}}\}$ and $\{\Delta\alpha = 0.78, r_{\mathrm{vo}} = 1.83 \ \mathrm{Gpc}, \Delta r = 0.03 r_{\mathrm{vo}}\}$, respectively. These values of r_{vo} correspond, in physical distances, to void sizes of 1.34 and 1.68 Gpc, respectively. We will also consider the so-called "constrained" model proposed in [4] which we will henceforth refer to as the "cGBH" model. For this model, we choose the parameters that maximize the likelihood as obtained in [4], which can be written in terms of α and β using (13) and (14). The main difference between the three models is that Model II features a much sharper transition from the void and that the cGBH model is almost twice as large. Nonetheless, neither transition width nor void size are expected to be important factors in cosmic parallax since in any case most quasars are outside the void and the most relevant quantity is the difference between the inner and outer values of H. In all three cases we set the off-center (physical) distance to 30 Mpc, which is the upper limit allowed by CMB dipole distortions (see Sec. II B), and this corresponds to $s \simeq 9 \times 10^{-3}$ for a source at $z = 1$.

Figure 2 depicts the behavior of $H_{\perp,0}$ and $H_{\parallel,0}$ as a function of the comoving distance from the center of the

FIG. 3 (color online).	Ω_{m0} for Model I (solid), Model II (dashed curve) and the cGBH model (red, long-dashed) as a function of the physical distance X. Note that the definition for Ω_{m0} we use differ from the one in [3,33,34] and we do not get their characteristic overdensity bump (or shell) surrounding the void.

void. Note that overall both functions are similar, specially outside the void (where they quickly approach 0.5). The main discrepancy is seen in $H_{\parallel,0}$ for Model II around the (sharp) transition region of the void. Similarly, Fig. 3 illustrates the void by depicting Ω_{m0} from the inside to the outside region, where it evaluates to unity.

In order to make better use of the FRW-like estimates in an LTB universe, one must first understand which H, parallel or transverse, corresponds to H_{obs} and H_X in (22). From (21) we get

$$X_{\mathrm{LTB}} = \int^r \frac{R'(t_0, r')}{\sqrt{1 + \beta(r')}} dr' \qquad (41)$$

and

$$\frac{\partial X}{\partial t} = \int^r \frac{\dot{R}'(t_0, r')}{\sqrt{1 + \beta(r')}} dr' \overset{\mathrm{eq.\ (2)}}{=} \int^r H_{\parallel}(t_0, r')$$

$$\times \frac{R'(t_0, r')}{\sqrt{1 + \beta(r')}} dr'. \qquad (42)$$

Therefore we write $\Delta X = (\partial X/\partial t)\Delta t + \mathcal{O}(\Delta t^2)$ and thus, defining $\bar{H}$ such that to first order $\Delta X \equiv X\bar{H}\Delta t$, we get

$$\bar{H} = \frac{1}{X} \int_0^r H_{\parallel}(t_0, r') \frac{R'(t_0, r')}{\sqrt{1 + \beta(r')}} dr'$$

$$= \frac{1}{\int_0^r \frac{R'(t_0,r')}{\sqrt{1+\beta(r')}} dr'} \int_0^r H_{\parallel}(t_0, r') \frac{R'(t_0, r')}{\sqrt{1 + \beta(r')}} dr'. \quad (43)$$

In a steplike LTB void model ($\Delta r \to 0$) the quantity H_X in (30) is given by

$$H_{\parallel}(t_0, r) = H_{\parallel}^{\mathrm{in}} + (H_{\parallel}^{\mathrm{out}} - H_{\parallel}^{\mathrm{in}})\Theta(r - r_{\mathrm{vo}}), \qquad (44)$$

where Θ is the Heaviside (or "step") function. Substituting in (43), we finally arrive at the sought after result $H_{\mathrm{obs}} = H_{\parallel,0}^{\mathrm{in}}$ and
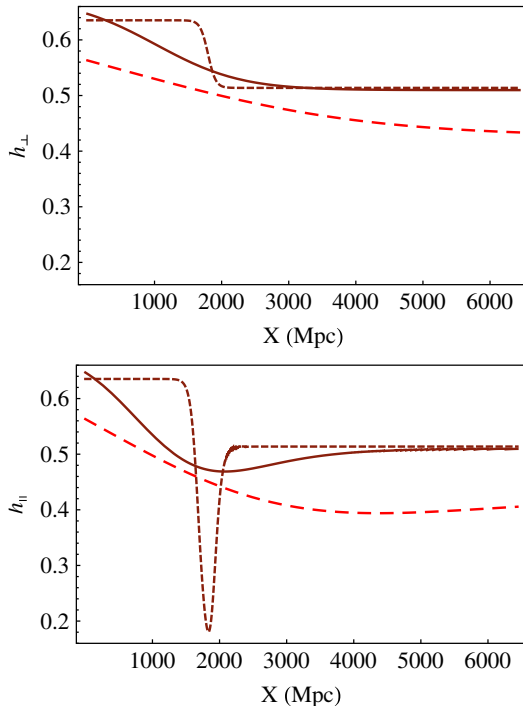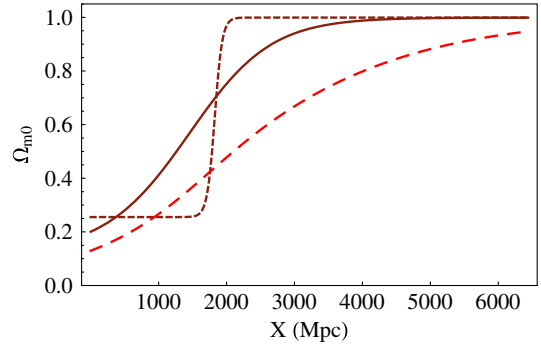

FIG. 2 (color online).	$H_{\parallel}$ and $H_{\perp}$ for Model I (solid), Model II (dashed curve) and the cGBH model (red, long-dashed) in units of $100 \ \mathrm{km}/(\mathrm{s}\,\mathrm{Mpc})$, as a function of the physical distance X. Note that both Hubble parameters differ only around the void-transition region.

$$\bar{H} = H_\parallel^{in}\frac{X_{vo}}{X} + H_{\parallel,0}^{out}\left(1 - \frac{X_{vo}}{X}\right) \simeq H_{\parallel,0}^{out}. \qquad (45)$$

This shows that in general, the values of H_{obs} and H_X in (30) are obtained by a combination of both $H_\parallel$ and $H_\perp$. On all three models here considered, however, these quantities differ by less than 30%. Since our main goal is to use (30) as an estimate of the true (numerical) effect, either one could be used. Nevertheless, in order to be as accurate as possible we shall [motivated by (45)], substitute H_{obs} and H_X by their LTB $H_\parallel$ counterparts.

D. The Sandage redshift drift

It has been known for a long time [16] that for any expanding cosmology the redshift z of a given source is not a constant in time. In a decelerating universe all redshifts decrease in time. In models predicting a recent (since $z \sim 1$) acceleration, like the ΛCDM model, sources with redshifts $z \lesssim 2$ actually have positive dz/dt. In effect, observation of dz/dt gives one a direct measurement of the expansion of the universe, and is at least in principle one of the few direct ways of measuring directly $H(z)$ (along with e.g. longitudinal acoustic oscillations). The prospect of doing so was revisited in [17].

If one assumes a FRW metric, the observed redshift of a given source, which emitted its light at a time t_s, is, today (t_0),

$$z_s(t_0) = \frac{a(t_0)}{a(t_s)} - 1, \qquad (46)$$

and it becomes, after a time interval Δt_0 (Δt_s for the source)

$$z_s(t_0 + \Delta t_0) = \frac{a(t_0 + \Delta t_0)}{a(t_s + \Delta t_s)} - 1. \qquad (47)$$

The observed redshift variation of the source is, then,

$$\Delta_t z_s = \frac{a(t_0 + \Delta t_0)}{a(t_s + \Delta t_s)} - \frac{a(t_0)}{a(t_s)}, \qquad (48)$$

which can be reexpressed, after an expansion at first order in $\Delta t/t$, as:

$$\Delta_t z_s = \Delta t_0\left(\frac{\dot{a}(t_0) - \dot{a}(t_s)}{a(t_s)}\right) + \mathcal{O}\left(\frac{\Delta t_0}{t_0}\right)^2. \qquad (49)$$

We can rewrite the last expression in terms of the Hubble parameter $H(z) = \dot{a}(z)/a(z)$:

$$\Delta_t z_s = H_0\Delta t_0\left(1 + z_s - \frac{H(z_s)}{H_0}\right). \qquad (50)$$

It will prove useful in Sec. IV, where we estimate achievable observational precision, to relate the redshift variation to an apparent velocity shift of the source, $\Delta v = c\Delta_t z_s/(1 + z_s)$.
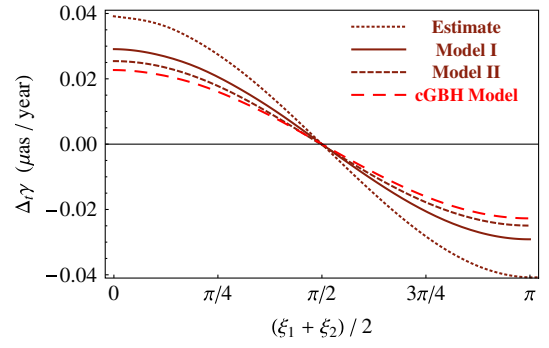

FIG. 4 (color online). $\Delta_t\gamma$ for two sources at the same shell, at $z = 1$, for Model I (full lines), Model II (dashed), the cGBH model (red, long-dashed lines) and the FRW-like estimate (dotted). The lines correspond to a separation of 90° in the sky between the sources. The off-center distance is assumed to be 30 Mpc.

This redshift drift, or $\dot{z}$, or "Sandage effect", has been investigated for a variety of dark-energy models currently pursued in the literature [37–40], and it is interesting to note that most of them predict a very similar redshift profile for the effect, all very close to the one generated by the ΛCDM model. In ΛCDM, the redshift drift is positive in the region $0 < z < 2.4$ but becomes negative for higher redshift (see Fig. 7). On the other hand, a dark-energy mimicking giant void produces a very distinct z dependence of this drift, and in fact one has, as we will show below, that dz/dt is always negative.[2]

E. Numerical results

In Fig. 4 we plot $\Delta_t\gamma$ for two sources at $z = 1$, for Models I and II as well as for the FRW-like estimate. One can see that the results do not depend sensitively on the details of the shell transition and that in both cases the FRW-like estimate gives a reasonable idea of the true LTB behavior. We conclude that (22) is indeed a valid approximation.

Figure 5 depicts the redshift dependence of the cosmic parallax effect for two sources at the same shell (i.e., same redshift) but separated in the sky by 90° (which is the average separation between two sources in an all-sky survey): one source is located at $\xi = -45°$, the other at $\xi = +45°$. Also plotted are the two major sources of systematic noise, which will be discussed in Sec. V: our own peculiar velocity and the change in the aberration of the sky due to the acceleration of the observer. As will be shown, all the effects we are considering are dipolar and the lines in Fig. 5 are proportional to the amplitudes of such dipoles. Note that both systematics have different z-dependence than the

---

[2]It has recently come to our attention that this property and its potential as discriminator between LTB voids and ΛCDM was first pointed out in [19].
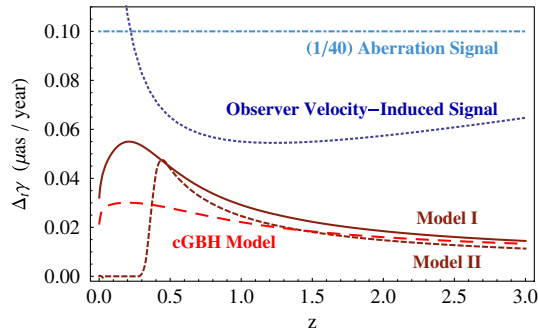
FIG. 5 (color online). $\Delta_t \gamma$ for two sources at the same shell but separated by 90° as a function of redshift assuming a 30 Mpc off-center distance. The dark, brown lines correspond to the cosmic parallax in Models I (full lines) and II (dashed); the red long-dashed lines to the cGBH model; the light, blue dotted lines represent 1/40 of the aberration-induced signal (see text), which does not depend on redshift; the dark dotted lines stand for the parallax induced by our own peculiar velocity (assumed to be 400 km/s). Since all effects are dipolar, the curves plotted here are proportional to the amplitude of such dipoles. The actual amount of noise depend on the angle between the center of the void and the directions of acceleration and peculiar velocity of the measuring instrument. Notice that as expected, in Model II the CP is zero inside the void.

CP produce in void models, and in principle all three effects can be separated.

As mentioned before, in principle the Sandage effect and cosmic parallax are two coupled effects and rigorously any calculation of one effect must take into account the other. Nevertheless, in practice the coupling is a weak one, and to compute the redshift drift one can always assume to good precision that the observer is in the center of the void. Figure 6 illustrates this fact by depicting the Sandage effect for a source at $z = 1$ as a function of the angle ξ for both Models I and II, for an observer 30 Mpc away from the
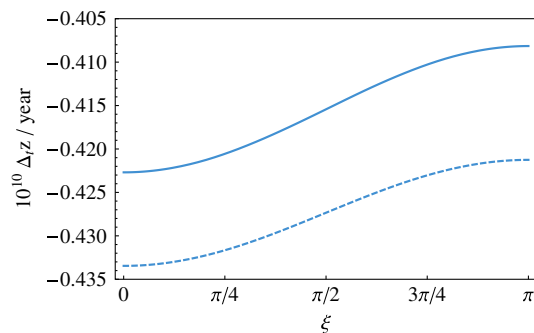

FIG. 6 (color online).   The Sandage effect for a source at $z = 1$ for an observer 30 Mpc away from the center as a function of the angle ξ for both Models I (full) and II (dashed lines). Note that the fractional fluctuation of the redshift drift in the sky is less than 5%, and one can therefore assume isotropy to good precision when computing this effect on void models.
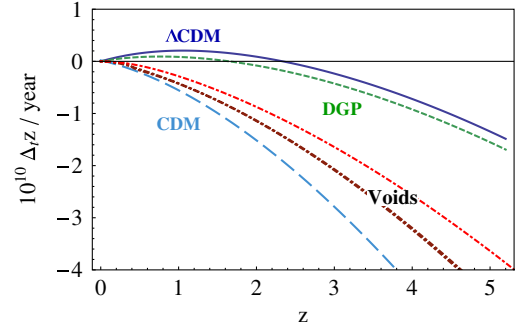

FIG. 7 (color online).   The annual redshift drift for different models assuming an observer at the center. The upper, blue solid lines represent the ΛCDM model. The green, dashed line corresponds to a self-accelerating DGP model with $\Omega_{r_c} = 0.13$. The dot-dashed lines stand for the 3 void models considered here: the dark brown (indistinguishable) lines are for Models I and II, while the red line just above correspond to the cGBH model. The bottommost line corresponds to an universe with only matter in a FRW metric (the CDM model). Note that the void models predict a curve which is in between CDM and ΛCDM but closer to the former.

center. As can be seen, the fractional fluctuation of the redshift drift in the sky is less than 5%.

Finally, Fig. 7 illustrates the Sandage effect as a function of redshift for ΛCDM the DGP model [41], the old matter dominated model (CDM) and the 3 different void models here considered. As could be expected, the void models predict a curve which is in between CDM and ΛCDM. Since the signal there is closer to the CDM one, this makes for a potentially powerful probe for distinguishing these dark-energy-like void models and ΛCDM, as we will see in detail in Sec. IV. Note that our results are in qualitative agreement with the ones obtained in [19].

IV. MEASURING THE REDSHIFT DRIFT WITH CODEX

Recently, two high-precision spectrographs were proposed which could in principle be used for measuring the redshift drift: the Cosmic Dynamics Experiment (CODEX) [24,39,40] at the European Extremely Large Telescope (E-ELT) [42] and the Echelle Spectrograph for PREcision Super Stable Observations (ESPRESSO) [39,40,43] at the Very Large Telescope array (VLT). Although proposed later, ESPRESSO would serve as a prototype implementation on the technology behind CODEX as part of its feasibility studies and could be operational several years before that experiment [39,40].

The possibility of detecting the redshift drift with CODEX was analyzed in a couple of papers [37–40]. In particular, it was shown in [38] that using reasonable mission specifications for CODEX, a discrimination amongst many different proposed dark-energy models would not be possible in a time-frame of less than 30 years.

Here we will show that void models, on the other hand, are much easier to tell apart through the Sandage effect than other dark-energy models. Using very similar mission specifications for CODEX, we estimate that a 5σ detection/exclusion is possible with less than 10 years of observation.

The achievable accuracy on $\sigma_{\Delta v}$ by the CODEX experiment was estimated (through Monte Carlo simulations) [24] to be

$$\sigma_{\Delta v} = 1.35\left(\frac{\text{S/N}}{2370}\right)^{-1}\left(\frac{N_{\text{QSO}}}{30}\right)^{-1/2}\left(\frac{1 + z_{\text{QSO}}}{5}\right)^q \text{ cm/s,} \tag{51}$$

with

$$q \equiv -1.7 \quad \text{for } z \le 4, \qquad q \equiv -0.9 \quad \text{for } z > 4, \tag{52}$$

where S/N is the signal-to-noise ratio per pixel, N_{QSO} is the total number of quasar spectra observed and z_{QSO} their redshift. Note also that the error prefactor 1.35 corresponds to using all available absorption lines, including metal lines; using only Lyα lines enlarges this prefactor to 2 [40].

The signal-to-noise ratio per pixel was estimated in [40] to be

$$\frac{S}{N} = 700\left[\frac{Z_X}{Z_r}10^{0.4(16-m_X)}\left(\frac{D}{42\text{ m}}\right)^2\frac{t_{\text{int}}}{10\text{ h}}\frac{\epsilon}{0.25}\right]^{1/2}, \tag{53}$$

where Z_X and m_X are the source zero point and apparent magnitude in the "X" band and D, t_{int} and ϵ are the telescope diameter, total integration time and total efficiency, respectively. We assumed a pixel size of 0.0125 Å and a central obscuration of the telescope's primary collecting area of 10% [40]. Note that $D = 42$ m corresponds to the reference design for the E-ELT [42].

The reason we quoted magnitudes in terms of an arbitrary "X" band is because one should use the magnitude of the bluest filter that still lies entirely redwards of the quasar's Lyα emission line [40]. This means that for $z_{\text{QSO}} < 2.2$ one should use the magnitude in the g-band; for $2.2 < z_{\text{QSO}} < 3.47$ the one in the r-band; for $3.47 < z_{\text{QSO}} < 4.61$ the i-band; for $z_{\text{QSO}} > 4.61$ the z-band. A good estimate for m_X can be achieved with the SDSS DR7, selecting the brightest quasars in each redshift bin using the appropriate band for such bin. Following [38] we will select 40 quasars in 5 redshift bins, centered at $z = \{2, 2.75, 3.5, 4.25, 5\}$, all of the same redshift width of 0.75. The corresponding bands are, in order, $\{g, r, r, i, z\}$ (where the i-band could equally be chosen for the middle bin). Doing so, one gets for the average (amongst the 8 brightest quasars) apparent magnitude m_X for each bin the following: $m_X = \{15.45, 16.54, 16.40, 17.51, 18.33\}$. Finally, we estimate the zero point magnitude ratio in each bin to be [44]: $Z_X/Z_r = \{1.01, 1.00, 1.00, 0.98, 0.93\}$. The accuracy of this last estimate is however quite unimportant in what follows.

One remark is in order before we proceed. In (51) it was tacitly assumed that the observational strategy concentrates all spectroscopic observations in the two endpoints of the interval Δt and that $t_{\text{int}} \ll \Delta t$. First of all, in order to obtain a good (> 2000) S/N with E-ELT, t_{int} is not negligible compared to Δt. Second, it has been claimed in [40] that in principle it would be preferable to spread the observations more evenly over Δt, although the same authors conclude that the best strategy to minimize the errors would be to concentrate as much as possible the telescope time in both the beginning and ending of Δt. Either way, the error estimate (51) is changed somewhat, but never by more than a factor 2. However, estimating such a correction depends on the details of the observational strategy and is beyond the scope of this work; therefore in what follows we will neglect this possibility.

Hereafter we will therefore assume a compromise strategy: a three-period observation, each of $\Delta t/3$ duration, and with observations contained in the first and third periods. Doing so means that the effective Δt for the Sandage drift is $2\Delta t/3$.[3] We will investigate three possible mission durations: 5, 10, and 15 years. It is important to note that a larger observational time-frame allows not only for a larger redshift drift (which is linear in time) but also for smaller error bars, as more photons are collected and, therefore, a higher S/N (which increases as $\sqrt{\Delta t}$) can be achieved. In other words, the "effective signal" increases with $\Delta t^{3/2}$ if one assumes a proportional telescope time is maintained.

Figure 8 depicts the Sandage effect for different dark-energy models for three possible (complete observation) time-spans: 5, 10 and 15 years. Also plotted are the forecasted error bars obtainable by CODEX at the E-ELT, the formula for which was discussed above. Here we are assuming that the time spent observing each quasar is the same, and this accounts for larger error bars at high redshift due to the lower apparent magnitudes of the corresponding quasars [see (53)]. Another possible strategy would be to increase the relative integration time for these sources in order to achieve the same average signal-to-noise ratio at all redshift bins. Table I contains the corresponding χ^2 and σ-levels for 5, 10 and 15 years. As can be seen, void models could be detected/ruled out at over 4σ with less than a decade of mission-time.

There is nothing special about the redshift binning proposed here. In fact, one could think about what would be the optimal redshift range for distinguishing between voids and ΛCDM. By inspection of Fig. 8, it seems that the "pivot redshift bin" is the third one, centered around

_____

[3]Although they do not explicitly mention what observational strategy they follow, it seems that the authors in [38] in fact overestimated the redshift drift signal by a factor of 2 by assuming the total time interval of observation (in their proposal, 30 years) to coincide with the time interval in the redshift drift signal. The latter, for observations taken evenly over Δt should in fact be half the former (15 years in their case).
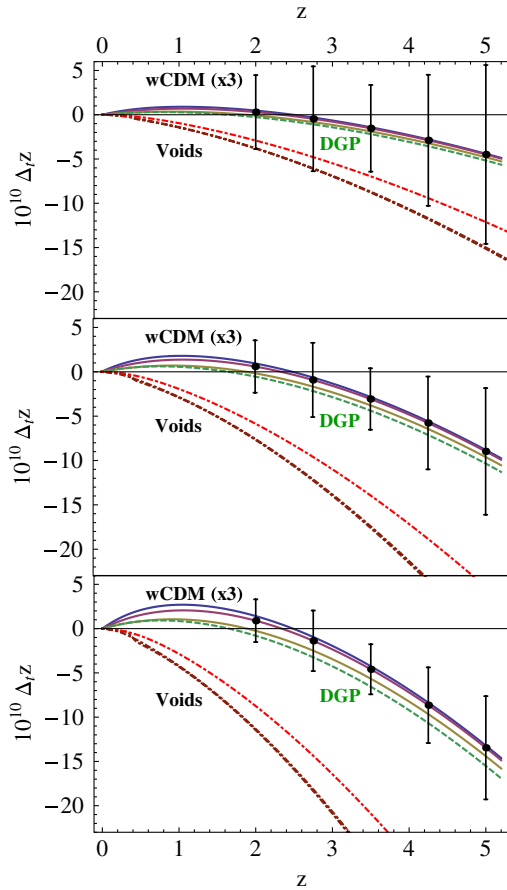
FIG. 8 (color online).   Redshift drift for different dark-energy models for a total mission duration of 5 (top), 10 (middle) and 15 (bottom plot) years and CODEX forecast error bars (the time-span between each measurement is 2/3 of that—see text). In each plot, the upper 3, solid lines represent wCDM models for $w = -1.25$ (uppermost), $w = -1$ (second) and $w = -0.75$ (third uppermost). The green, dashed line corresponds to a self-accelerating DGP model with $\Omega_{r_c} = 0.13$. The three bottommost, dot-dashed lines stand for the 3 void models considered here: the dark brown (indistinguishable) lines are for Models I and II, while the red line just above correspond to the cGBH model. Note that a 4σ separation between voids and ΛCDM can be achieved in a decade.

$z = 3.5$. The reason is that this is the best compromise between the difference in the signal between the void and ΛCDM (which increase with z) and quasar brightness (which decrease with z). In fact, if we only use the 8

TABLE I.   Estimated achievable confidence levels by the CODEX mission in 5, 10, and 15 years.

Model	5 years	10 years	15 years
Models I/II	1.1σ	6.2σ	12.5σ
	$\chi^2 = 6.5$	$\chi^2 = 52$	$\chi^2 = 176$
cGBH Model	$.5\sigma$	4.3σ	9.2σ
	$\chi^2 = 3.7$	$\chi^2 = 30$	$\chi^2 = 100$

QSOs in that bin we could improve the detection levels to $\{1.8\sigma, 8.0\sigma, 15.7\sigma\}$ for Models I or II in $\{5, 10, 15\}$ years. However, this might not be desirable for two reasons: first, the pivot bins for other dark-energy models are likely to be different; second, using more than a handful of quasars is important to wash out possible systematics, and actually for the SDSS catalog, using 40 QSOs all around $z = 3.5$ *decreases* the detection levels compared to the proposed binning (to $\{0.8\sigma, 5.3\sigma, 11.0\sigma\}$ for the Models I or II) because we are then forced to use some not-so-bright quasars.

One very interesting aspect of using the Sandage effect to probe void models is the fact it is model-independent to a good degree. In fact, although in the cGBH model the signal is a little smaller, both Models I and II here studied never differ by more than 0.1σ and except for tiny differences close to the void edge (barely resolvable in Fig. 8), they both predict the very same redshift drift profile. These models should be good representatives of this whole class of these dark-energy mimicking LTB void models. Model I is very smooth, Model II represents an abrupt change between "inside" and "outside" the void and the cGBH model represents one of the largest (over 2 Gpc) voids in the literature.

In the next section we focus on the other real-time observable, cosmic parallax.

V. MEASURING THE COSMIC PARALLAX WITH GAIA

Distance measurements are one of the most fundamental challenges in astronomy. The simplest and historically more important method to measure cosmic distances relies on parallaxes, i.e., the apparent change in position of an object relative to some reference frame generated by a known displacement of the observer. In all astronomical applications these displacements are small compared to the distances of the source: the lunar parallax is around 1 degree; planetary parallaxes[4] are $\lesssim 11$ arcsec; stellar parallax are $\lesssim 1$ arcsec; galactic parallaxes[5] are $\lesssim 1$ μas. Therefore measuring parallaxes of distant sources require enough precision to detect tiny angular changes in position. Even though observation of parallaxes on supergalactic scales are daunting, of all (large) distance measurements they present the least amount of systematics. This is the main reason why astrometry has recently reacquired an important role among the ground-based and space-based planned missions. Measuring a possible apparent change in the relative position of cosmological sources like quasars

---

[4]Lunar and planetary parallaxes are measured from two different points on the surface of the Earth, and therefore have a baseline limited by our planet's diameter.

[5]Stellar and galactic parallaxes are measured from two different positions along the orbit of the Earth around the Sun, and therefore have a maximum baseline of 2 AU.

in any anisotropic expansion scenario, dubbed in [20] cosmic parallax, is one of the next challenges for astrometry.

In particular, missions that perform *global astrometry* over the entire celestial sphere are preferred because: (i) increasing the number of measurement helps increasing the required accuracy; (ii) cosmic parallax is an all-sky effect, the multipole expansion of which depend on (and therefore is a signature of) the underlying anisotropic model. Such programs measure the positions of objects relative to other objects separated by a large angle on the sky, such that they have a different parallactic effect. Therefore these missions demands the capability to survey large and complete (flux-limited) sample of objects. In ground-spaced programs the observations are typically done over a small field of view. In addition, the choice of going to space offers the usual advantages of a stable thermal environment, freedom from gravity and the atmosphere, and full-sky visibility. This factors enable the high-precision wide-angle astrometry as implemented on missions such as Gaia [25,26] and SIM Lite Astrometric Observatory [27,28].

Gaia is an European Space Agency (ESA) mission that will be launched in 2012 with a nominal duration of 6 years. It marks a significant step forward in astrometry, moving into the era of microarcsecond astronomy and greatly extending Hipparcos' capabilities. The goal is to achieve an astrometric accuracy (for the positional error σ_p) between 10 μas (for sources with magnitude 15 on the G band) and 140 μas (for $G = 20$) [25] (although the final accuracy may be lower according to a revised estimate in [45]), which should be compared to Hipparcos' 1000 μas astrometry and limiting magnitude of 12. Gaia will also produce a full-sky map of roughly 0.5–1.0×10^6 quasars and 10^9 stars down to its limiting magnitude of $G = 20$, whose positions will be determined (on average) with the above accuracy. Direct optical observations of quasars is an important aspect of Gaia. These will be observed in all of its 15 photometric bands at 100 epochs from which the classes of quasars and their variability may be studied. The relevance of measuring quasars is heightened due to the fact that a fraction of them will be used to define the reference frame with respect to which the positions of all other objects will be compared.

The observing strategy for Gaia (a drifting sky-scan) is not optimal for observing the CP, which would benefit from maximizing the time interval between quasar observations. However, even if the observational program does not take into account the CP, in any case it constitutes at least a systematic that should not be ignored as it enlarges the astrometric error of any global-astrometry mission.

A rough estimate of the quasar distribution that Gaia is expected to see comes from the observations made by the Sloan Digital Sky Survey (SDSS) [46]. An earlier (pre-SDSS) but more adequate estimate on this distribution was

made in [47] running a simulation using Gaia's parameters, but using the I instead of the G band. The mission's target astrometric accuracy as a function of magnitude was derived in [25]. Figure 9 depicts these forecasts as a function of the magnitude in the G band. The plotted quasar distribution was obtained through the Sky Server [48] using the seventh data release (DR7) of SDSS, which in the magnitude range of Gaia encompasses nearly 100000 quasars. Combining these predictions allows us to estimate the average positional precision of Gaia on quasars by taking a simple weighted average: 102 μas (with the projection in [47]) or 82 μas (SDSS-like distribution). Based on these predictions we shall henceforth assume an average precision of 90 μas.

To compare our observations to Gaia we need to evaluate the average $\Delta_t \gamma$ with $\Delta t = 6$ years and N sources. The average angular separation of random points on a sphere is $\pi/2$ and thus the average of $\Delta_t \gamma$ can be estimated simply as $\Delta_t \gamma(\theta = \pi/2)$. The final Gaia error σ_p is obtained by best-fitting $2N$ independent coordinates from $N^2/2$ angular separation measures; the average positional error on the entire sky will thus scale as $(2N)^{-1/2}$. The error scales therefore as $\sigma_p/\sqrt{2N_{QSO}}$. Since the CP signal increases linearly with time, it is convenient to define

$$\sqrt{N_{QSO}}\left(\frac{\Delta t}{1 \text{ year}}\right)\left(\frac{\sigma_p}{1 \ \mu\text{as}}\right)^{-1}, \tag{54}$$

which makes for a good figure-of-merit (FOM) for cosmic parallax measurements. In the definition above, Δt is the average time interval between the two measurement epochs, and σ_p is the average positional astrometric accuracy achieved *in each epoch*. With $N_{QSO} = 5 \cdot 10^5$ and 90 μas, Gaia's FOM is 39. With a million sources, the FOM increases to around 55. In the Appendix B we show
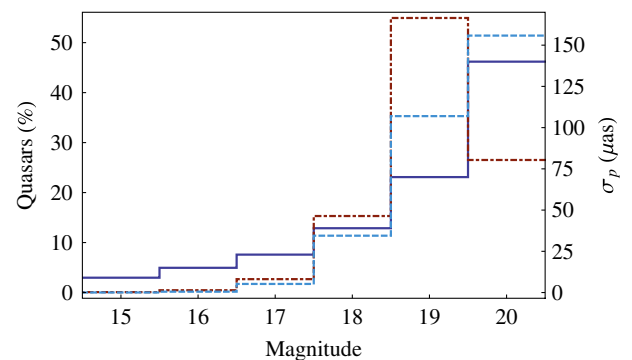

FIG. 9 (color online). Target Gaia astrometric accuracy (dark, full lines) and projected quasar distribution (light, dashed) as a function of magnitude in the G and I band, respectively. Also plotted is the quasar distribution obtained using SDSS DR7 (red, dot-dashed), plotted against its own G band magnitude. A simple weighted average gives the typical positional precision of Gaia on quasars: either 102 μas (projected) or 82 μas (SDSS-like distribution).

that, as a cosmic parallax measuring mission, SIM Lite is less promising than Gaia, boasting a FOM of only 9.

Figure 10 illustrates the possibility of detecting the cosmic parallax with Gaia for a possible, though arbitrary, redshift binning. Depicted are $\Delta_t\gamma$ for two sources at the same shell for both Models I (full) and II (dashed lines) and for a time span of 10 (top), 20 (middle) and 30 (bottom plot) years, together with Gaia forecast statistical error bars. The error bars are given by

$$\langle\sigma_p\rangle/\sqrt{2N_{QSO}} \qquad (55)$$

in each bin, where $\langle\sigma_p\rangle$ is Gaia's magnitude-averaged precision on the corresponding bin. These errors correspond to the previous nominal mission duration of 5 years and assume the SDSS-like quasar distribution (see Fig. 9). An extension to 10 or more years allow smaller error bars and here too we can approximate the errors to scale as
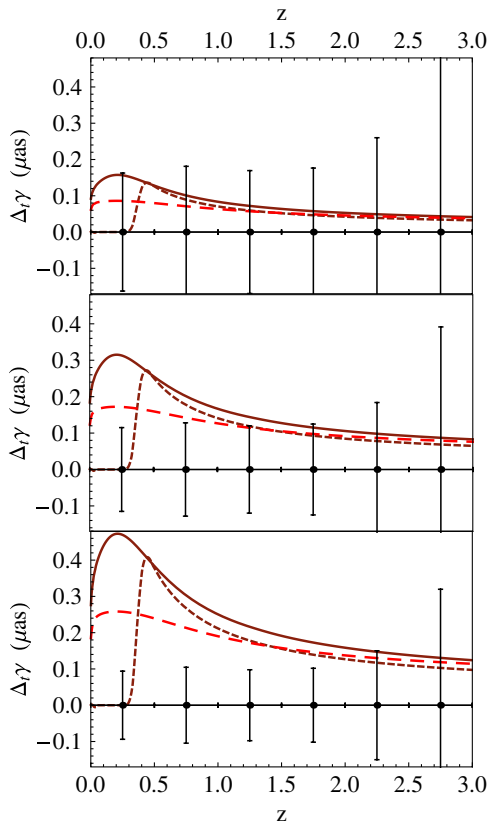
TABLE II. Estimated achievable confidence levels by the Gaia (or an extended Gaia-like) mission in 10, 20, and 30 years, in the limit where the two considered systematics are arbitrarily distinguished apart. For the Gaia's nominal duration of 6 years, detection levels are essentially zero.

Model	10 years	20 years	30 years
Model I	$.05\sigma$	1.8σ	4.9σ
	$\chi^2 = 1.4$	$\chi^2 = 11$	$\chi^2 = 39$
Model II	$.003\sigma$	$.5\sigma$	2.2σ
	$\chi^2 = .5$	$\chi^2 = 4.3$	$\chi^2 = 19$
cGBH Model	$.005\sigma$	$.6\sigma$	2.6σ
	$\chi^2 = .6$	$\chi^2 = 5$	$\chi^2 = 17$

$(\Delta t)^{-1/2}$. For $z > 3$, the error bars get much larger and the CP is quite small, so that higher-z bins do not add much. Here we are not considering the two main source of systematics identified below. As in Fig. 5, the lines correspond to a separation of 90° in the sky between the sources, which is the average separation between any two sources in the sky. Table II contains the corresponding χ^2 and σ-levels.

Let us now come back to the matter of the fiducial off-center distance, raised in Sec. II B. We have so far assumed such a distance to be 30 Mpc, which is the largest distance in agreement with the CMB dipole for an observer without peculiar velocity. Since the cosmic parallax signal is directly proportional to such a distance, one could also phrase the argument of detection in a different way. If we ignore the CMB dipole (and all other) dipolar-anisotropy constraints and leave the off-center distance as a free parameter, how well could Gaia constrain it? To estimate this one need only calculate, for a given number of mission years, what is the off-center distance that would produce a 1σ detection. Table III summarizes the results for all 3 models in 6, 10, 20, and 30 years. Interestingly, although a Gaia-like mission requires around 20 years to reach the constraining level of the CMB dipole, already with 6 years it is an equivalent or even better probe of dipolar anisotropy in comparison to current supernovae data sets, which only limit such a distance to around 200–400 Mpc depending on the model [35].

Clearly, the Gaia mission with its nominal duration of 6 years cannot detect the cosmic parallax in void models. For a longer mission duration, however, detection (say, 3σ)

FIG. 10 (color online). $\Delta_t\gamma$ for two sources at the same shell for both Models I (full) and II (dashed lines) and for a time span of 10 (top), 20 (middle), and 30 (bottom plot) years, together with Gaia forecast statistical error bars. Although the nominal Gaia duration is only 6 years, a mission extension allow for smaller errors. Here we are not considering the two main systematics identified in the text. The lines correspond to the average cosmic parallax effect over the whole sky which is given by (25). Note that the CP quickly becomes the best probe of present anisotropy and, therefore, of the combination of distance and velocity towards the center of a void.

TABLE III. Estimated off-center distance constraints (in Mpc) from the Gaia (or an extended Gaia-like) mission in 6, 10, 20, and 30 years, in the limit where the two considered systematics are arbitrarily distinguished apart.

Model	6 years	10 years	20 years	30 years
Model I	143	66	23	13
Model II	235	109	39	21
cGBH Model	214	99	35	19

could be in principle achieved with less than the 30 years estimated in Table II. The reason is twofold. First, earlier estimates for Gaia hinted to the possibility of detecting up to 1×10^6 quasars, which is twice the value we are considering here. This extra data, if confirmed, would amount to an extra 2σ to the detection levels in 30 years in any of the three models. Second, we only considered here a simplified strategy of binning quasars in redshift, which amounts to comparing the cosmic parallax of sources at same distances. But in principle one should also compare quasars at different redshifts, and this could lead to an average higher signal. Finally, one should also take into account the ϕ-coordinate in the distribution of the quasars, and doing so should change the estimates somewhat. We leave the last two points, however, for future work.

It is important to note that, although Gaia uses a fraction of the quasars to self-calibrate its inertial reference frame, these are only used to correct for rotations, which is a basically independent degree of freedom. In other words, all observed quasars can be used to reduce the errors statistically [49].

Two local effects induce spurious parallaxes (the observation of which are interesting on its own): one (of the order of 0.1 μas/year) is induced by our own peculiar velocity[6] and the other (of the order of 4 μas/year [50]) by a changing aberration[7] due to the observers' acceleration. In astronomy in general (and cosmic parallax is no exception) a possible constant aberration is irrelevant. However, since the Sun is accelerating towards the center of the Milky Way, the resulting change in aberration does produce a competing signal which must be distinguished. This acceleration is the dominant competing effect, and even though the orbit around the galaxy is not circular, the extra yearly aberration due to this acceleration is given by the familiar centripetal acceleration formula [50] $a_{SUN} = V_{rot}^2/R_{SUN}$. Current uncertainties on these two (sometimes called fundamental) parameters are around 5–10% [52], but radio astrometry at the Very Long Baseline Array (VLBA) might bring these down to 1% within one decade [53], which would imply around 3% precision in a_{SUN}. Although this could in principle be used to predict and therefore subtract 97% of this changing aberration, amounting to a residual signal of approximately 0.1 μas/year, such a procedure is not necessary: the best way to tell apart aberration effects from cosmic parallax is through their distinct redshift dependence (see Fig. 5).

Both changing aberration and our own peculiar velocity produce a dipolar parallax signal, just like in LTB. However, as per our comments following (32), the peculiar velocity parallax decreases monotonically with the angular diameter distance (but not with redshift), while the aberration residual noise is *independent of distance*. In contrast, the LTB signal has a characteristic nontrivial dependence on redshift: for the models investigated here it is either moderate (Model I) or vanishingly small (Model II) inside the void, large near the edge and decreasing at large distances (see Fig. 5). It is therefore in principle possible to separate the cosmic signal from the (residual) local ones, for instance estimating the local effects from sources inside the void. In fact, Milky Way stars form a gravitationally bound system and are not subject to cosmic parallax. They can therefore be used to self-calibrate Gaia and help separate the aberration-induced signal. A detailed calculation of the detection levels obtainable by Gaia requires not only taking these two systematics into account, but also a careful simulation of experimental settings (including possibly effects like source photocenter jitter and relativistic light deflection by solar system bodies) which is outside the scope of this paper.

One final note regarding these systematics: more general (non-LTB) anisotropic models will not produce a simple dipole [22,23] and their cosmic parallax can be more easily distinguished from local effects.

VI. CONCLUSIONS

In this paper we have presented two methods to map large-scale inhomogeneity and late-time anisotropy: the redshift drift and cosmic parallax, respectively. Together, these real-time observables can fully reconstruct the 3D cosmic flow of distant sources. We forecasted the effect induced by a large void centered, or nearly centered, on the Milky Way, and, in particular, we have shown that the two effects can be detected with the E-ELT and with Gaia or an enhanced version of Gaia. The two effects add to the limited number of tests that can be employed to distinguish a LTB void from an accelerating FRW universe, possibly eliminating an exotic alternative explanation to dark energy.

In LTB void models, the Sandage effect turns out to be mostly sensitive to the scale of the void, but not to other particular void properties like steepness of the transition. The CP, on the other hand, being basically an anisotropy probe is mostly sensitive to the off-center distance, and in fact should be zero for on-center observers. It also depends somewhat on the particular void profile, specially for $z \lesssim 0.5$. Nevertheless, although one can guess this low-z (inside the void) CP behavior for pathological cases like the very abrupt Model II (where it is zero, as per Figs. 5 and 10), it is not obvious how exactly all the void parameters enter into the final effect.

It turns out that the best hope to attain a clear-cut discrimination between LTB and FRW is with the redshift drift effect, since the LTB expansion is always decelerated. We find that a 4σ separation can be achieved with E-ELT in

---

[6]Since the void is not expect to be moving with respect to the quasars frame, the peculiar velocity signal should be understood as one between our local group and the center of the void.

[7]Aberration is an optical distortion effect in the sky whenever observer and sources have nonzero relative velocities (see, for instance, [51]).

less than 10 years, much before the same experiment will be able to distinguish between competing models of dark energy. A Gaia-like mission, on the other hand, can only achieve a reasonable detection of a void-induced cosmic parallax in the course of 30 years.

Nevertheless, cosmic parallax remains an important tool and in fact one of the most promising way to probe general late-time cosmological anisotropy, as already discussed in [20,23]. In particular, even if it only lasts 6 years Gaia should constrain late-time anisotropies similarly to current supernovae catalogs, but in an independent way. Also, in ΛCDM it can be used to measure our own peculiar velocity with respect to the quasar reference frame and consequently to the CMB, therefore providing a new and promising way to break the degeneracy between the intrinsic CMB dipole and our own peculiar velocity. We are currently investigating this possibility and results will be published in a subsequent paper.

Direct kinematic tests as redshift drift and cosmic parallax are conceptually the simplest probe of expansion and of anisotropy since their interpretation do not rely on calibration of standard candles/rulers nor depend on evolutionary or selection effects (as for galaxy ages and number counts). The fact that in both CP and redshift drift the "effective signal" increases as $(\Delta t)^{3/2}$ shows that these new real-time cosmology effects can become some of the most effective long-term dark-energy probes. For the same reason, the Sandage and cosmic parallax effects have also the potential to become the best inhomogeneity and (late-time) anisotropy tests, respectively. Combined, they will form an important direct test of the FRW metric.

Although the odds of Gaia having fuel to last 10 or more years are small, one can consider Gaia as making a first sub-miliarcsecond astrometric sky-map, which could be confronted with any future global-astrometry mission. Since any proper motion signal increases linearly with time, any future mission with a global astrometric accuracy *at least* as good as Gaia can be used to detect the CP (or any other kind of late-time anisotropy) signal. In between missions, however, the effective signal grows only linearly in Δt.

It is really exciting that two great tools like Gaia and E-ELT are becoming reality just now when we begin to realize the importance of extremely precise astrometric and spectroscopic measurements for cosmology.

APPENDIX A: NUMERICAL NUANCES

The intrinsically smallness of both the cosmic parallax and Sandage effects demand a carefully constructed numerical code to correctly compute either. As stated before, a straightforward calculation of $\Delta_t \gamma$ per year requires evaluating ξ_{a1} and ξ_{a2} with at least 15 orders of precision (as the CP is of order 0.2 μas/year $\sim 10^{-13}$ rad/year).

It is possible to alleviate this by exploiting the linearity of $\Delta_t \gamma$ in Δt and scaling up the system. In fact, we confirmed that such linearity held at least up to $\Delta t = 10^6$ years, so that this was the value used in [20] to compute the CP, dividing in the end the result by 10^6 to get the parallax-per-year. However, even for such an enlarged time span, a CP estimation still require an end-of-calculation precision of 9 digits; for the stated algorithm, which involves solving 5 coupled differential equations many times and comparing the results, this is not possible using standard double-precision techniques.

The first method we resorted to used a simplification for the metric. In the limit $|\alpha(r)\beta(r)/R(t, r) \ll 1|$ (which always holds in the models we investigated), the metric $R(t, r)$ can be written explicitly [54] without resort to the parameter η. This allowed us to further exploit arbitrary-precision numerical routines such as the ones found in Mathematica© to carry on our computations with a precision higher than the regular machine-precision (16 digits of precision). Surprisingly, even though the metric approximation is very reasonable, the results obtained were not consistent. This is probably due to the fact that second derivatives appear in (35) (a good approximation to a function might not be so for its derivatives) and also to

the fact that the stated algorithm is very sensitive to any small deviations to the geodesics' paths.

Therefore we dropped the approximation in [54] in favor of another one: setting R_{lss} to zero in (39) and (40). This has negligible impact on the metric for $z \lesssim 10$. Doing so allows us to invert (10) and obtain the function $\eta[2\beta(r)^{3/2}t/\alpha(r)]$ and its first 2 derivatives using Mathematica's arbitrary-precision routines, thus computing the metric to a high-enough precision in order to obtain consistent results. Since going above machine precision slows down any code exponentially we must also be careful not to set the target precision too high. Over different parts of the algorithm we had to work with in between 20 and 30-digit precision.

Even when using high-precision techniques, numerical noise became unstable whenever $\beta(r)$ became too close to zero [as can be easily seen through (9) and (10)], so we adopted a slightly modified version of (40):

$$\beta(r) = (H_{\perp,0}^{out})^2 r^2 \frac{\Delta \alpha}{2}\left(1.001 - \tanh\frac{r - r_{vo}}{2\Delta r}\right), \quad (A1)$$

where the only change was on the factor before the tanh from 1 to 1.001. Does this affect the CP signal? We tested this for both Models I and II by putting a higher factor of either 1.01 or 1.05 and found out that there is no change in any results, so we assume the same should hold in the limit where this factor goes to unity.

APPENDIX B: MEASURING THE COSMIC PARALLAX WITH SIM LITE

The SIM Lite Astrometric Observatory (a smaller, cost effective version of the formerly known SIM PlanetQuest) [27,28] is being developed by the Jet Propulsion Laboratory under contract with NASA and has a target launch-date for around 2016. Like Gaia, it is also a astrometry-centered mission with a 5-year nominal duration, but one with different observational strategy and scientific goals. One of its main objectives is the search for Earth-sized extrasolar planets and therefore instead of pursuing a global astrometric measurement it will focus on specific regions of the sky. In these narrow regions, SIM Lite can achieve a higher precision compared to Gaia: 1 μas with a single measurement and 4 μas for the global astrometric grid. Nevertheless as we will show below, SIM Lite is less adequate than Gaia for measuring the cosmic parallax, mostly due to the small amount of time devoted to extragalactic observations. In fact, current proposals call for an observation of only 50 quasars, devoting only 1.5% of the mission duration for that purpose.

How does SIM Lite compare with respect to Gaia in measuring the cosmic parallax? As discussed in Sec. V, the precision of such measurement scales as $\sigma_p/\sqrt{N_{QSO}}$. For Gaia, as shown, we estimate $\sigma_p = 90$ μas and at least $N_{QSO} = 500000$; for SIM Lite, $\sigma_p \approx 4$ μas and $N_{QSO} = 50$ (a selected sample with magnitude in the R band less than 16.5 [28]). Therefore the CP figure-of-merit (see Sec. V) of SIM Lite is 9, which is over 4 times smaller than Gaia's FOM (which is 39). Nevertheless, SIM Lite only allocates 1.5% of its mission time to observing quasars. One could therefore question how much better could a similar instrument do in observing the CP if it allocated 100% of its time for that purpose. A first estimate would then give $N_{QSO} \approx 3000$ (a realistic number, as SDSS DR7 contains a little over 1000 quasars with $R < 16.5$), and in this case such a mission would have around double the precision (i.e., FOM) of Gaia. Since clearly Gaia's CP-measuring capabilities could also be enhanced on a similar way by allocating more integration-time for quasars, it remains the most promising current proposal for that.

---

[1] N. P. Humphreys, R. Maartens, and D. R. Matravers, Astrophys. J. **477**, 47 (1997).

[2] M.-N. Célérier, Astron. Astrophys. **353**, 63 (2000).

[3] H. Alnes, M. Amarzguioui, and O. Gron, Phys. Rev. D **73**, 083519 (2006).

[4] J. Garcia-Bellido and T. Haugboelle, J. Cosmol. Astropart. Phys. 04 (2008) 003.

[5] K. Tomita, Astrophys. J. **529**, 38 (2000).

[6] M.-N. Célérier, K. Bolejko, A. Krasiński, and C. Hellaby, arXiv:0906.0905v1.

[7] T. Biswas and A. Notari, J. Cosmol. Astropart. Phys. 06 (2008) 021.

[8] V. Marra, E. W. Kolb, S. Matarrese, and A. Riotto, Phys. Rev. D **76**, 123004 (2007).

[9] K. Kainulainen and V. Marra, Phys. Rev. D **80**, 127301 (2009).

[10] L. Amendola, M. Quartin, S. Tsujikawa, and I. Waga, Phys. Rev. D **74**, 023525 (2006).

[11] M. Quartin, M. O. Calvão, S. E. Joras, R. R. R. Reis and I. Waga, J. Cosmol. Astropart. Phys. 05 (2008) 007.

[12] M. H. Partovi and B. Mashhoon, Astrophys. J. **276**, 4 (1984).

[13] N. Mustapha, C. Hellaby, and G. F. R. Ellis, Mon. Not. R. Astron. Soc. **292**, 817 (1997).

[14] J. Garcia-Bellido and T. Haugboelle, J. Cosmol. Astropart. Phys. 09 (2008) 016.

[15] R. R. Caldwell and A. Stebbins, Phys. Rev. Lett. **100**, 191302 (2008).

[16] A. Sandage, Astrophys. J. **136**, 319 (1962).

[17] A. Loeb, Astrophys. J. **499**, L111 (1998).

[18] J.-P. Uzan, C. Clarkson, and G. F. R. Ellis, Phys. Rev. Lett. **100**, 191303 (2008).

[19] C.-M. Yoo, T. Kai, and K. Nakao, Prog. Theor. Phys. **120**, 937 (2008).

[20] C. Quercellini, M. Quartin, and L. Amendola, Phys. Rev. Lett. **102**, 151302 (2009).

[21] F. Ding and R. A. C. Croft, Mon. Not. R. Astron. Soc. **397**, 1739 (2009).

[22] M. Fontanini, M. Trodden, and E. J. West, Phys. Rev. D **80**, 123515 (2009).

[23] C. Quercellini, P. Cabella, L. Amendola, M. Quartin, and A. Balbi, Phys. Rev. D. **80**, 063527 (2009).

[24] L. Pasquini, S. Cristiani, H. Dekker *et al.*, The Messenger **122**, 10 (2005).

[25] M. A. C. Perryman *et al.*, Astron. Astrophys. **369**, 339 (2001).

[26] C. A. L. Bailer-Jones, in *IAU Colloq.*, edited by D. W. Kurtz (Cambridge University, Cambridge, 2005), Vol. 196, pp. 429–443.

[27] R. Goullioud, J. H. Catanzarite, F. G. Dekens, M. Shao, and J. C. Marr IV, arXiv:0807.1668.

[28] SIM Lite Astrometric Observatory, J. Davidson, S. Edberg, R. Danner, B. Nemati and S. Unwin (editors), (2009); http://planetquest.jpl.nasa.gov/SIM/keyPubPapers/simBook2009/.

[29] S. Alexander, T. Biswas, A. Notari, and D. Vaid, J. Cosmol. Astropart. Phys. 09 (2009) 025.

[30] T. Clifton, P. G. Ferreira, and K. Land, Phys. Rev. Lett. **101**, 131302 (2008).

[31] S. February, J. Larena, M. Smith, and C. Clarkson, arXiv:0909.1479v1.

[32] C. Clarkson, B. Bassett, and T. H.-C. Lu, Phys. Rev. Lett. **101**, 011301 (2008).

[33] H. Alnes and M. Amarzguioui, Phys. Rev. D **74**, 103520 (2006).

[34] H. Alnes and M. Amarzguioui, Phys. Rev. D **75**, 023506 (2007).

[35] M. Blomqvist and E. Mortsell, arXiv:0909.4723v1.

[36] C. Lineweaver, Moriond Astrophysics 1996, 69 (1996).

[37] P.-S. Corasaniti, D. Huterer, and A. Melchiorri, Phys. Rev. D **75**, 062001 (2007).

[38] A. Balbi and C. Quercellini, Mon. Not. R. Astron. Soc. **382**, 1623 (2007).

[39] S. Cristiani *et al.*, Nuovo Cimento Soc. Ital. Fis. B **122** 1159 (2007); , 1165 (2007).

[40] J. Liske, A. Grazian, E. Vanzella *et al.*, Mon. Not. R. Astron. Soc. **386**, 1192 (2008).

[41] G. R. Dvali, G. Gabadadze, and M. Porrati, Phys. Lett. B **485**, 208 (2000).

[42] R. Gilmozzi and J. Spyromilio, Messenger **127**, 11 (2007).

[43] V. D'Odorico (the CODEX/ESPRESSO team), arXiv:0708.1258v2.

[44] B. Fornal, D. L. Tucker, J. A. Smith, S. S. Allam, C. J. Rider, and H. Sung, Astron. J. **133**, 1409 (2007).

[45] L. Lindegren *et al.*, *Proceedings of the International Astronomical Union* (IAU Symposium, Cambridge, 2008), Vol. 248, pp. 217–223.

[46] D. G. York *et al.*, Astron. J. **120**, 1579 (2000).

[47] http://www.rssd.esa.int/SA-general/Projects/GAIA_files/LATEX2HTML/report.html.

[48] SDSS Sky Server: http://cas.sdss.org/dr7.

[49] L. Lindegren (private communication).

[50] J. Kovalevsky, Astron. Astrophys. **404**, 743 (2003).

[51] M. O. Calvão, G. I. Gomero, B. Mota, and M. J. Rebouças, Classical Quantum Gravity **22**, 1991 (2005).

[52] M. J. Reid *et al.*, Astrophys. J. **700**, 137 (2009); J. Bovy, D. W. Hogg, and H.-W. Rix, Astrophys. J. **704**, 1704 (2009); P. J. McMillan and J. J. Binney, arXiv:0907.4685v1.

[53] M. J. Reid, K. M. Menten, A. Brunthaler, and G. A. Moellenbrock, arXiv:0902.3928.

[54] D. J. H. Chung and A. Enea Romano, Phys. Rev. D **74**, 103507 (2006).